Myosin Orientation in a Muscle Fiber Determined with High Angular Resolution Using Bifunctional Spin Labels

Yahor Savich[1,2], Benjamin P. Binder[1,3], Andrew R. Thompson[1], and David D. Thomas[1*]

[1] *Department of Biochemistry, Molecular Biology and Biophysics, University of Minnesota, Minneapolis, MN 55455*
[2]*School of Physics and Astronomy, University of Minnesota, Minneapolis, MN 55455*
[3]*Department of Chemistry, Augsburg University, Minneapolis, MN 55454*

Summary: We used electron paramagnetic resonance to determine the orientation of elements within the myosin regulatory light chain in skinned skeletal muscle fibers. A bifunctional spin label provided sufficient resolution to detect an ordered population of lever arms perpendicular to actin.

*To whom correspondence should be addressed: ddt@umn.edu

Keywords: electron paramagnetic resonance, muscle, BSL, myosin, RLC

ABSTRACT We have measured the orientation of the myosin light chain domain in demembranated muscle fibers by electron paramagnetic resonance (EPR), using a bifunctional spin label (BSL), with angular resolution of 4 degrees. Despite advances in X-ray crystallography, cryo-electron microscopy (cryo-EM), and fluorescence polarization, none of these techniques provide high-resolution structural information about the myosin light chain domain under ambient conditions in fiber. Two cysteines, 4 residues apart, were engineered on an α helix in the myosin regulatory light chain (RLC), permitting stereoselective site-directed labeling with BSL. By exchanging BSL-labeled RLC onto oriented muscle fibers, we obtained EPR spectra that resolved angular distributions in several biochemical states. The accurate determination of BSL's angular coordinates allowed us to determine the orientation of individual structural elements with respect to the muscle fiber axis. The addition of ATP, in the absence of Ca^{2+}, shifted the orientation to a much more disordered distribution. We resolved an oriented population with lever arm oriented perpendicular to the muscle fiber axis, a state previously observed directly in insect flight muscle, but not in fibers having isolated myosin heads (S1) attached to actin.

INTRODUCTION

Muscle contraction is a process in which the nanometer-sized force-bearing elements of myosin contribute to macroscopic tissue contraction. Despite recent technical advances in cryo-EM and X-ray crystallography, important structural details of the mechanism of force generation by myosin remain unclear. The essential light chain (ELC) and regulatory light chain bind to an α-helix on the myosin heavy chain (MHC), forming the light-chain domain (LCD), which acts as a lever arm for producing force and movement. Either due to structural flexibility of this complex, or to ensemble or sample inhomogeneity, the above methods have not definitively determined the structure of the LCD, even in the simplest biochemical state – rigor (no ATP). In addition, none of the above-mentioned structural techniques provide structural information under physiological conditions (not frozen or crystallized) in muscle fibers. Fluorescence polarization does not have this limitation, and has been used to provide some orientational information about the ELC (Knowles et al., 2008) and RLC (Brack et al., 2004; Romano et al., 2012; Fusi et al., 2015) in skinned fibers. However, fluorescence has low angular resolution, so this approach requires data from multiple labeling sites and complex data analysis.

Electron paramagnetic resonance (EPR) of nitroxide spin labels offers high orientational resolution (1–5 degrees) under physiological conditions, which is needed to overcome the above limitations (Thomas and Cooke, 1980; Cooke et al., 1982; Arata, 1990; Thomas et al., 2009; Mello and Thomas, 2012; Thomas et al., 2012; Nogara et al., 2016). The sensitivity of the EPR spectrum to the angle between the nitroxide's π orbital (z_N-axis in Fig. 1B) and the magnetic field $\vec{B}$ (light blue arrow in Fig. 1B), and to the rate and amplitude of rotational motion, provides high-resolution information about the orientation and rotational motion of a spin label relative to the magnetic field. The BSL (Fig. 1) provides rigid and stereospecific attachment of the probe to an α helix (Fleissner et al., 2011), thus providing unambiguous information about helix orientation (with ~1 degree resolution) and rotational motion, as demonstrated previously in applications to actin-bound myosin (Arata et al., 2003; Rayes et al., 2011; Binder et al., 2015; Thompson et al., 2015; Binder et al., 2018). Due to increasing interest in thick filament muscle regulation, it is important to study both the actin-attached and actin-unattached states of myosin with BSL's high angular resolution, given that the orientation of the LCD in multiple biochemical states in contracting muscle remains ambiguous (Irving, 2017).

In the present study, we exchanged BSL-labeled RLC onto the myosin lever arm in permeabilized rabbit muscle fiber bundles, and measured the orientation of helices in the N- and C-lobes in the absence of nucleotide (rigor) and in the presence of ATP (relaxation).

METHODS

Protein and muscle fiber preparations

Mutants of rabbit skeletal RLC (skRLC) and chicken gizzard smooth muscle RLC (smRLC) were obtained by site-directed mutagenesis, expressed in E. coli, and purified as previously described (Nelson et al., 2005). Endogenous cysteines were replaced by alanines, and a di-cysteine BSL labeling motif was introduced for each construct on the following helices: B (D53C-A57C), E (G103C-V107C) in skRLC and B (D56C-S60C) in smRLC. Skinned rabbit psoas muscle fiber bundles were dissected and permeabilized as described previously (Prochniewicz et al., 2008) and stored in Fiber Storage Buffer with 4mM DTT added. Rabbit skeletal heavy meromyosin (HMM) was purified as described in (Muretta et al., 2015).

Preparation of BSL-RLC

Di-Cys RLC mutants in labeling buffer (30mM Tris, 50mM KCl, 3mM $MgCl_2$, pH 7.5) were incubated at 4°C with 5mM DTT for 1hr to ensure reduction of engineered cysteine residues prior to labeling. DTT was removed using Zeba Spin desalting columns (Thermo Scientific), and RLC was incubated at 4°C for 1hr in 5-fold molar excess of bifunctional 3,4-Bis-(methanethiosulfonylmethyl)-2,2,5,5-tetramethyl-2,5-dihydro-1H-pyrrol-1-yloxy spin label (BSL; Toronto Research Chemicals). Following incubation, excess spin label was removed and the protein was exchanged into rigor buffer (25 mM Imidazole, 10 mM EGTA, 100.3 mM KPr, 1.5 $MgAc_2$, pH 7.1) using Zeba Spin desalting columns.

BSL-RLC exchange onto HMM and decoration of fiber with BSL-RLC-HMM.

BSL-labeled RLC was exchanged onto HMM (Muretta et al., 2015) by combining the two proteins (3:1 RLC:HMM, mol/mol) in 50 mM Tris pH 7.5, 120 mM KCl, 12 mM EDTA. Samples were incubated for 10 minutes at 30°C, followed by addition of 12 mM $MgCl_2$ and incubation on ice for 15 minutes. Free RLC was subsequently removed using Amicon Ultra Centrifugal Filters, 0.5 mL, 50K MWCO (EMD Millipore), and finally samples were exchanged into rigor buffer. Fiber bundles were decorated by the resulting BSL-RLC-HMM complex by circulating protein samples through a 25 µL Drummond glass capillary (Drummond Scientific) with a tied fiber bundle.

BSL-RLC exchange into permeabilized fibers.

Glycerinated rabbit psoas fibers were dissected into bundles, ranging from 0.3-0.5 mm in diameter and 3-5 cm in length, and were tied at each end using surgical silk. The tied fiber bundles were then held in place at a fixed length within a 25 µL Drummond glass capillary (Drummond Scientific), with the ends of the sutures being affixed to the capillary using short sections of silicone tubing. Buffer exchange was accomplished with a Masterflex C/L peristaltic pump (Cole-Parmer) at the flow rate of 0.5 mL/min. Exchange of BSL-labeled RLC constructs onto permeabilized fibers was done following previously developed methods (Mello and Thomas, 2012) with the exception that the concentration of DTT in the wash before the acquisition was 0.5 mM (instead of 30 mM incubation). Rigor and relaxation solutions used during acquisition were as described in (Fusi et al., 2015).

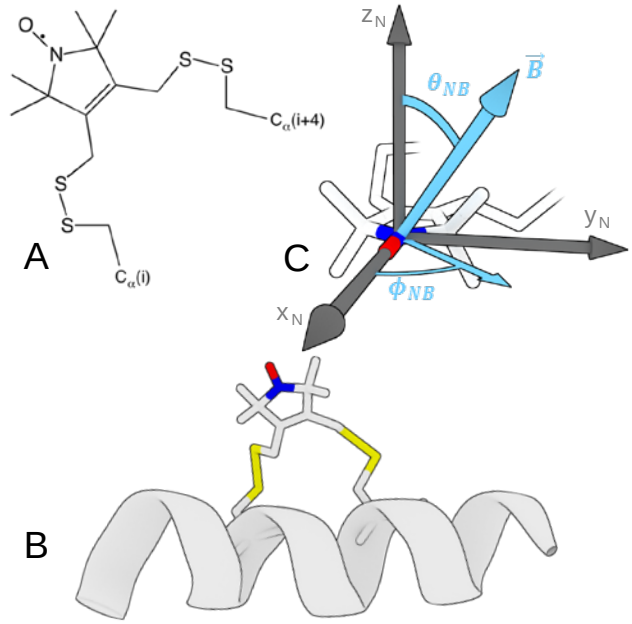

Fig. 1. (A) The chemical structure of BSL (3,4-Bis-[methanethiosulfonylmethyl]-2,2,5,5-tetramethyl-2,5-dihydro-1H-pyrrol-1-yloxy spin label) reacted with the two Cys residues. (B) BSL bound stereospecifically to an α-helix at positions i and i+4. (C) Angles that define the orientation of the nitroxide (defined by axes x_N , y_N , z_N) relative to the applied magnetic field $\vec{B}$; these angles directly determine the orientation dependence of the EPR spectrum (Thompson et al., 2008; Binder et al., 2015; Thompson et al., 2015).

Ionic strength and pH during acquisition were kept at 150 mM and 7.1, respectively.

EPR spectroscopy

EPR was performed on a Bruker EleXsys E500 X-band spectrometer ($\nu = 9.6$ GHz). Spectra of BSL-RLC and BSL-RLC-HMM were acquired in an ER4122 SHQ spherical resonator. Parallel and perpendicular field experiments on fiber bundles were performed in TM_{110} 4103TMA and TE_{102} 4104OR-R resonators, respectively. Minced fiber measurements were performed in a quartz flat cell in the TE_{102} 4104OR-R cavity. Sample temperature was set to 4ºC in all experiments. Sweep width was 120 G with 1024 points per spectrum. The center magnetic field (B_c) was set according to $B_c = \nu/2.803\ MHz/G$. Conversion time and time constant were set to 20.48 ms. Modulation amplitude and microwave power were 1-2 G and 2-20 mW, depending on the cavity.

Data analysis

EPR spectra were background-subtracted, normalized by dividing by the second integral and analyzed as described previously to determine the angular distribution of spin labels relative to the muscle fiber axis, assuming the rigid limit regime due to the immobilization granted by the BSL spin label (Binder et al., 2015). Magnetic tensor values (g and T, defining the orientational dependence of the spectrum) were determined from completely disordered samples (minced fibers). The angular distribution was fit to Gaussian functions for both angles θ_{NB} and ϕ_{NB}, (Fig. 1C), with full width at half-maximum (FWHM) $\Delta\theta$ and $\Delta\phi$. Sensitivity of EPR to θ_{NB} in systems with an axial symmetry (as with oriented

muscle fibers) is considerably greater than the sensitivity to ϕ_{NB}, so in this study we only use θ_{NB} values for molecular modeling. Confidence intervals were determined from the cumulative distribution function of the F-ratio distribution comparing the ratio of the residual sum of squares of the fits with the residual sum of squares of the best fit.

Molecular modeling

Angle measurements derived from atomistic models were calculated using custom extensions written for Visual Molecular Dynamics 1.9.3 (VMD) (Humphrey et al., 1996). Minimization of models was performed with help from the SciPy and NumPy packages of the Python Programming Language. Structure images were rendered using Blender, Version 2.79 (Blender Foundation).

RESULTS

Detecting anisotropy in the EPR fiber experiment and RLC homolog comparison.

There are three types of measurements for studying muscle using EPR: (1) parallel, (2) perpendicular field experiments with the fiber parallel, perpendicular to the magnetic field respectively, and (3) minced fiber experiment, in which the any orientational order (i.e. anisotropy) of the fiber system is removed. In the presence of anisotropy in a biological sample, the parallel spectrum line shape (Fig. 2A, magenta) will show the biggest difference from the minced fiber measurement (Fig. 2A, green), which is an isotropic control. The perpendicular field experiment is sensitive to orientation (Fig. 2A, orange), but not in a straightforward, qualitative way, considering the helical symmetry of the actomyosin complex about the muscle fiber axis. For the sake of simplicity, in the subsequent discussion of fiber experiments we only show the parallel experimental data.

Our previous work on myosin in skeletal fiber bundles and HMM involved smooth muscle RLC (smRLC) from chicken gizzard (Mello and Thomas, 2012; Muretta et al., 2015). We tested our protocol with skRLC homolog. Fig. 2B shows that θ_{NB} orientations of smRLC and skRLC are hardly distinguishable, which is consistent with fluorescence polarization experiments (Romano et al., 2012). Therefore, to maximize the physiological relevance of our work, we focused on skRLC from here on.

BSL is immobilized on the RLC and attached stereospecifically.

The rotational correlation time of the spin label in the conventional EPR experiment is given by $\tau_R = a\left[1-\left(\frac{T'_{\parallel}}{T_{\parallel}}\right)\right]^b$, where $2T'_{\parallel}$ is the splitting between the low- and the high-field features of the observed spectrum (Fig. 4), $2T_{\parallel}$ is the rigid-limit splitting (69-71 G, depending on local polarity), while $a = 5.4\times10^{-10}s$ and $b = -1.36$ are empirically determined parameters (Goldman et al., 1972). $2T'_{\parallel}$ of the isolated BSL-RLC constructs in solution does not depend on the label position (Fig. 4, blue) and is measured to be 67.6 ± 0.2 G, corresponding to a correlation

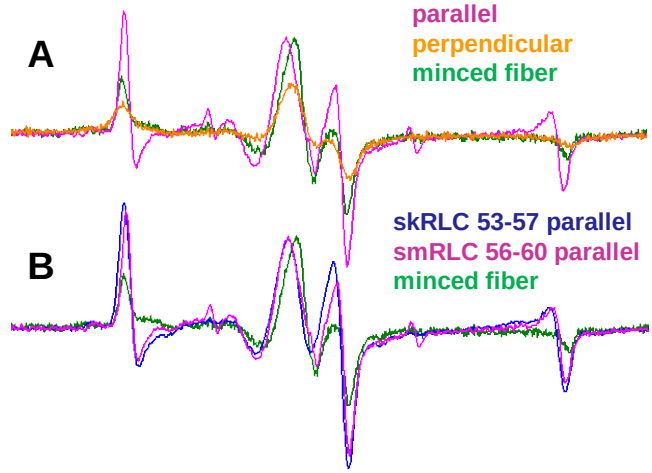

Fig. 2. (A) The effect of changing fiber orientation on EPR spectrum for smRLC helix B (56-60). **(B)** The parallel field experiment on helix B of skRLC and smRLC homologs labeled at equivalent sites.

time of 30-60 ns, consistent with the expected rapid tumbling of the isolated RLC in solution. Exchanging BSL-RLC (MW 19,000) onto HMM (MW 350,000) leads to an increase of $T'_{\parallel}$ (Fig. 4, black) to the range expected for the rigid limit, for probes attached to both the B helix and E helices. We conclude that BSL is rigidly immobilized when bifunctionally attached to RLC. This is consistent with the rigid and stereospecific immobilization seen previously with BSL attached to other proteins (Thompson et al., 2008; Thompson et al., 2015; Her et al., 2018).

Orientation of the probes in fiber bundles

Following the RLC-fiber exchange protocol, we performed EPR measurements on helices B and E. They yielded a significant oriented component in rigor (compare blue and green on Fig. 3Fig. 5A). With a single Gaussian oriented component, the B helix in the N-lobe was fit by $(\theta_{NB}, \Delta\theta) \approx$ (4.3°, 20°) and the E helix in the C-lobe was fit by $(\theta_{NB}, \Delta\theta) \approx$ (81.3°, 27°) (Fig. 3C, blue). Changing rigor buffer to a relaxation solution, the 20º and 27º distributions disappear, and the spectra become very similar to the minced fiber line shape (compare red and green on Fig. 3B). Confidence intervals were determined from the cumulative distribution function of the F-ratio distribution comparing the ratio of the residual sum of squares of the fits with the residual sum of squares of the best fit. The intervals of 95% are depicted by horizontal lines (insets, Fig. 3A). Thus uncertainty of the fit of the orientation of the probes on the B and E helices were determined to be ≈ 4°.

Helices B and E are oriented in fiber bundle experiments, but only helix E remains oriented in BSL-RLC-HMM-decorated fibers

The specificity of the RLC exchange onto HMM has been confirmed in our previous studies (Muretta et al., 2015; Rohde et al., 2017), however a non-specific binding of RLC to demembranated fibers can obscure the measurement of orientation (Mello and Thomas, 2012) or might lead to an inconclusive data interpretation. To ensure that the measured orientation in a fiber bundle stems from the RLC specifically bound to the IQ domain of actin-attached myosin, we exchanged BSL-RLC onto HMM. After decorating a fiber

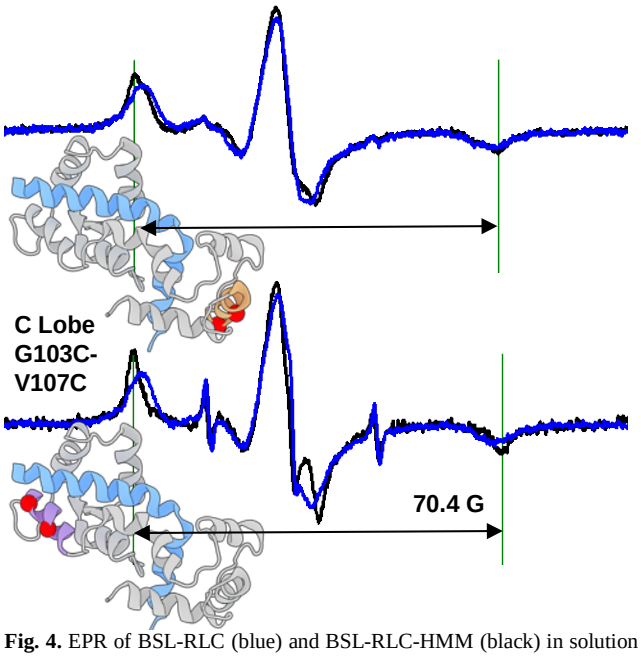

Fig. 4. EPR of BSL-RLC (blue) and BSL-RLC-HMM (black) in solution (randomly oriented). Inserts under spectra show RLC in grey with a fragment of myosin heavy chain in blue. Position of label is depicted by red spheres on B-helix (orange) of N-lobe and E-helix (magenta) of C-lobe.

bundle with BSL-RLC-HMM, we measured EPR while perfusing the bundle with rigor buffer. The line shape of the E helix in the BSL-RLC-HMM-fiber experiment stays similar to the BSL-RLC-fiber data (Fig. 5, bottom), reporting $\theta_{NB} \approx 81°$, with some differences in Lorentzian/Gaussian broadening and intensity. The B helix does not have any signatures of orientation (compare blue and black, Fig. 5, top). We proceeded by performing molecular modeling of the actin-attached state in the absence of nucleotide with the orientational distributions from (Fig. 3C, blue).

Model of a lever arm in a nucleotide-free state.

Having determined orientational distributions of BSL on the B and E helices of the RLC, we sought to compare those measurements with established atomic models of the actomyosin complex. We began with a recent cryo-EM structure derived from rabbit skeletal muscle (PDB: 5H53) (Fujii and Namba, 2017) which used the squid 3I5G crystal structure for docking and refinement of myosin coordinates. Coordinates for BSL were obtained from a crystal structure of the label bound to a helix in T4 lysozyme (Fleissner et al., 2011). BSL was modeled onto both experimental RLC sites by alignment of backbone atoms, with the orientation of each label adjusted to reflect conformational refinements from recent EPR studies (Binder et al., 2015). A θ_{NB} value was subsequently calculated from the model for each label, with the model's actin filament axis assumed to be parallel to the external magnetic field (as it would be in a parallel-oriented fiber experiment). Initial results gave poor agreement with the orientational distribution centers derived from our EPR data: θ_{NB} for Helix B was 37.1° (difference of +33.1°), and θ_{NB} for Helix E was 70.4° (difference of -10.6°) (Fig. 5C, blue).

This initial result was not surprising, as (1) the myosin captured in 5H53 structure was not resolved in the lever arm domain, and (2) the structure is of frozen myosin S1, and thus the LCD, might have a very different orientation than measured in our EPR experiments with HMM and full-length myosin in an *in situ* demembranated fiber bundle. Therefore, we sought to find the orientation of the myosin LCD that best accommodates the measurements derived from EPR.

We began by aligning additional myosin S1 structures to our actomyosin model, choosing several structures solved in various biochemical states with different LCD orientations (Houdusse et al., 2000; Himmel et al., 2002), (Fig. 6). Next, we used an established method to calculate a vector corresponding to the LCD helix in each structure (Enkhbayar et al., 2008), and subsequently found the approximate center of rotation for the LCD by calculating the average point of nearest convergence for all vectors (Fig. 6). Next, we applied a series of arbitrary 3D rotations

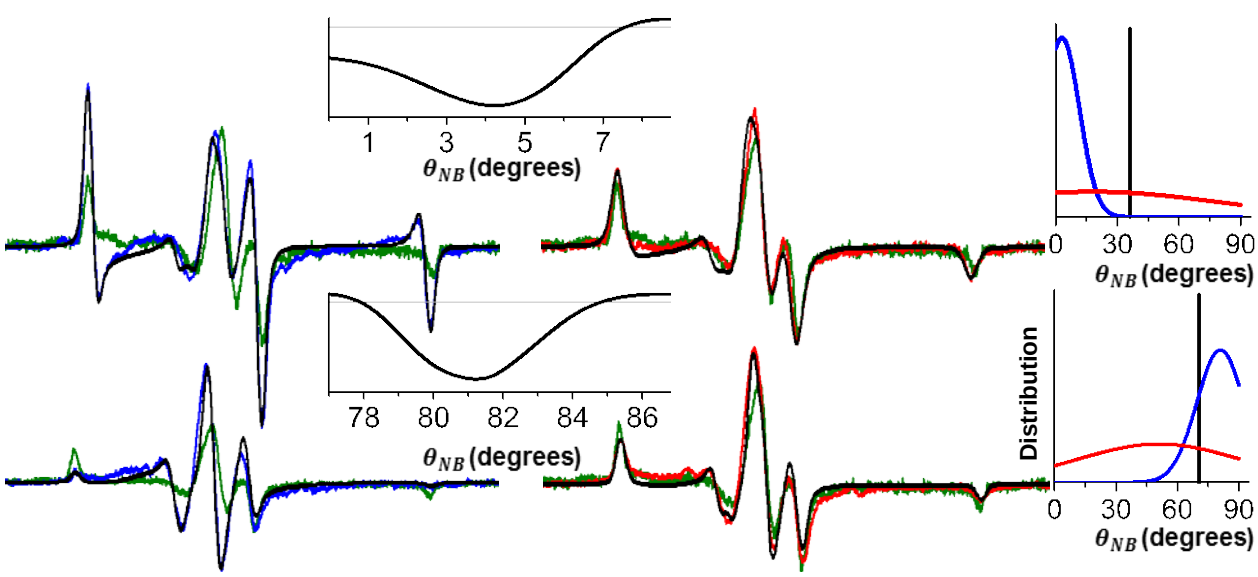

Fig. 3. EPR of BSL-RLC-fiber in **(A)** rigor (blue) and **(B)** relaxation (red). Fits are in black and the minced fiber data (isotropic control) is green. Insets in **(A)** represent projection of the error surface to θ_{NA}. 95% confidence intervals are depicted by a horizontal line. The θ_{NA} distribution in **(C)** for nucleotide-free (blue) and ATP-bound (red) state, derived from corresponding helices. Vertical bars represent predicted angles from the (PDB: 5H53) model.

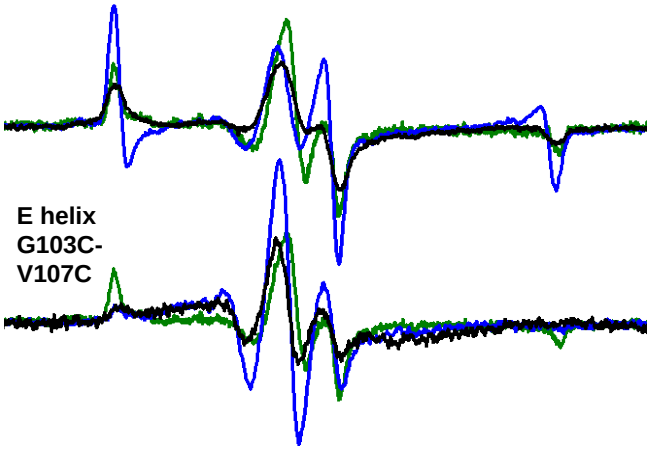

Fig. 5. EPR spectra of BSL-RLC-HMM-fiber (black) and BSL-RLC-fiber (blue) in parallel orientation. Minced BSL-RLC-fiber as an isotropic control is in green.

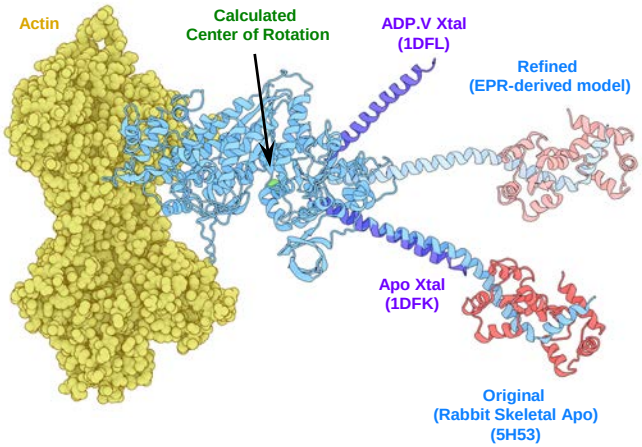

Fig. 6. Refinement of the rigor actomyosin model. In blue: the initial model of skeletal myosin attached to actin (yellow) with RLC in red (5H53). Catalytic domains of myosin in other states were aligned with the catalytic domain of 5H53 to find the plane of lever arm rotation (purple) – 1DFL and 1DFK (Houdusse et al., 2000). Center of rotation is denoted by a green sphere. In pale blue: lever arm orientation derived from EPR-derived orientations of helices B and E on the RLC (pale red).

about that defined center to the portion of our model comprising the LCD, RLC, and attached labels. After each transformation, we calculated new θ_{NB} values from the model, and assessed their deviation from the corresponding EPR-derived measurements. Minimizing these deviations by least-squares optimization yielded a new orientation of the LCD that is compatible with our experimental findings (Fig. 6).

While there are of course many potential 3D rotations that could bring the angles into agreement, the structure depicted in (Fig. 6) represents the solution that renders the smallest possible perturbation on our initial cryo-EM-based model. The optimal rotation relative to the starting structure is parameterized by Euler angles α = 0°, $\beta = -33.2°$, and γ = +3.3°, in the model's global coordinate space using the ZYZ-convention. The small magnitude of both α and γ indicate minimal azimuthal rotation relative to the actin axis, which was oriented along the global z-axis in our model. While the β value indicates a significant alteration in the LCD tilt relative to actin, it is striking to observe that this EPR-informed solution falls within the same rotational plane as the LCD's in other atomic structures of S1 (Fig. 6). We will refer to this rotational plane as the "powerstroke plane" in subsequent discussion. We also applied the above procedure to a structure of chicken skeletal myosin (PDB ID: 2MYS). In the 2MYS model, our labeling sites correspond to E49C-A53C and G99C-V103C. The search for an EPR-compatible rotation of the LCD converged on a configuration with α = 0°, β = -48.7°, and γ = +20.2°. Thus, not only did the 2MYS-based rotation consist of much more drastic adjustments than were rendered on 5H53, but it also places the lever arm significantly outside of the power-stroke plane. Hence, the smallest structural adjustment of the lever arm accommodating our data is a rotation α = 0°, β = -33.2°, and γ = +3.3°, which brings 5H53 lever arm down to a more perpendicular orientation (Fig. 6).

DISCUSSION

Summary of Results

We used BSL to determine the orientation of specific structural elements of skeletal muscle myosin. We studied BSL-labeled fiber bundles in three configurations – parallel to the magnetic field, perpendicular to the magnetic field, and minced (randomly oriented) (Fig. 2A). We found that smRLC, used in previous studies (Mello and Thomas, 2012), reports similar orientation compared to skRLC, consistent with previous results (Romano et al., 2012).

BSL has been previously shown to adopt a highly stereospecific conformation on protein α-helices (Binder et al., 2015; Binder et al., 2018). In the present study, we found that BSL was strongly immobilized when bound to the RLC helices (Fig. 4). Since our angular predictions for demembranated fiber bundles did not agree with S1 5H53 cryo-EM model data, we found a minimum rotation of the myosin lever arm which brings it to agreement with our angular parameters (Fig. 6). The rotation turns out to be a myosin state with lever arm perpendicular to muscle axis.

The N-lobe of RLC is less immobilized than the C-lobe in HMM

Assuming that the motion of the B and E helices of the RLC represent the motion of N- and C- lobes correspondingly, we see drastically different behavior of RLC lobes in HMM. The C-lobe displays twofold stronger immobilization than the N-lobe, as seen in our HMM experiment in solution (Fig. 4). Upon decorating fiber bundles with labeled HMM, the E helix reports an orientation of $\theta_{NB} \approx 81^{o}$ between the magnetic field and the probe – very similar to the BSL-RLC-fiber result (Fig. 5, bottom). In contrast, the N-lobe showed no orientation. (Fig. 5, top)

We hypothesize that this behavior is observed because the N-lobe is closer to a free coiled-coil motif. This hypothesis is supported by the observation that the shape of EPR spectrum for that lobe depends slightly on the buffer flow rate, which is not the case for samples in which we observe strong immobilization.

Comparison with fluorescence polarization data

To better contextualize our modeling results, we made comparisons with recent fluorescence anisotropy measurements (Romano et al., 2012). In that previous work, the authors defined a "lever axis" as a vector joining the α-carbons of Cys707 and Lys843 of the 2MYS model. They also defined a "hook axis" as a vector joining the midpoints between Phe836/Ile838 and Met832/Leu834 of the same model. Orientation of the LCD was characterized by β (the angle between the lever axis and actin), and γ (rotation of the hook axis around the lever axis). Romano and colleagues reported a maximum entropy distribution centered at (β, γ) ≈ (105º, 40º). By setting (β, γ) of 2MYS with BSL probes attached to E49C-A53C and G99C-V103C, we were able to directly compare these two methods. The above-mentioned rotation puts θ_{NB} of the B and E helix to 14.6º and 85.3º, respectively. Thus, the result of (Romano et al., 2012) lies within the confidence interval of our method, whereas orientation of the B helix differs from ours by 10.3º. Even though fluorescence anisotropy experiments are versatile in measuring changes of orientation with high temporal resolution, one should not forget that maximum entropy distribution is a low-resolution approximation of the actual angular distribution, thus the difference in 10.3º could be attributed to multiple factors.

Oriented rigor population of myosin with lever arm perpendicular to actin

Previous scallop muscle EPR measurements (Baker et al., 1998) showed at least a 30º LCD rotation during isometric contraction, while smRLC EPR experiments (Mello and Thomas, 2012) showed at least a 13º LCD rotation between the rigor and pPDM state (which resembles the pre-power stroke state). Since both of these studies used a monofunctional spin label, lacking explicit coupling between the probe orientation and that of the helix to which it is attached, it is not possible to describe more precise lever arm orientation (as we have done here with BSL) beyond changes in orientation.

Despite the limitations of EPR to predict atomic models, there is some evidence that the lever arm occupies a more perpendicular state in the post-power stroke state. EM tomography on insect flight muscle (Schmitz et al., 1996; Chen et al., 2002) shows populations of cross-bridges with more perpendicular lever arm orientation than is predicted by 5H53. Perpendicular conformation of a myosin lever arm was found in two types of cross-bridges: 1) lead bridge 2) back bridge. The lead bridge is a double-headed cross-bridge in a myac layer (longitudinal section containing a single layer of alternating actin and myosin filaments). The myosin molecule that is closer to M-line (M-ward lead bridge head) is fitted by a "lever down" model (tilt angle $151° \pm 1.1°$). The myosin molecule that is closer to the Z-disk however (Z-ward lead bridge head) has a tilt angle of $98° \pm 2.3°$. The back bridge is a single headed cross-bridge with a lever arm tilt of $106° \pm 12°$. We hypothesized, that our EPR derived model (Fig. 6) represents either Z-ward lead bridge head or a rear bridge. A characteristic property of the rear bridge EM density is that it disappears under nucleotide addition, e.g. AMPPNP (Schmitz et al., 1996). Addition of AMPPNP, however, does not change the angular distribution in our case (SI). Thus, we suggest that our oriented population of myosin represent Z-ward heads of the lead bridge. In the EM tomography analysis, group averaging was performed over self-similar motifs. This method prevents averaging-out of ordered populations in a sample with a high degree of heterogeneity. Similarly, the analysis of EPR spectra is mostly centered on the features of narrow orientational distributions.

Finally, fast skeletal muscle consists of 25% of myosin with a short ELC isoform (ELC-A2) that binds more weakly to actin and has been shown to induce a more perpendicular lever arm orientation the apo state (Guhathakurta et al., 2015). The high degree of orientational disorder present in all 6 constructs might suggest that we are seeing a minor ordered population similar to that reported in (Guhathakurta et al., 2015). Performing this research in a cardiac system might shed light on this hypothesis, since cardiac muscle has only one ELC isoform.

CONCLUSION

In this study, we characterized the actin-attached state of myosin without a nucleotide - rigor. We found a $\approx 33°$ rotation of the lever arm that accommodates the angular distributions of BSL. The rotation is happening in the powerstroke plane, which was previously observed in insect flight muscle. A plethora of other nucleotide states and conditions are accessible for study with this method, which will be addressed in the future.

AUTHOR CONTRIBUTIONS

All authors participated in the experimental design. YS performed the research and analyzed the data. BPB performed molecular modeling. YS, BPB, ART, and DDT wrote the paper. All authors approved the final version of the manuscript.

ACKNOWLEDGEMENTS

We thank Malcolm Irving's group, Kenneth Taylor, and Dawn Lowe for fruitful discussions, D. Grant Lewis for assistance with HMM experiments, and Octavian Cornea for administrative assistance. EPR experiments were performed at the Biophysical Technology Center, University of Minnesota. This study was supported by National Institutes of Health (NIH) grants R01AR032961 and R37AG26160 to DDT. YS was supported by NIH T32AG29796 and by a University of Minnesota Interdisciplinary Doctoral Fellowship.

REFERENCES

Arata, T. 1990. Orientation of spin-labeled light chain 2 of myosin heads in muscle fibers. *J Mol Biol*. 214:471-478. doi:10.1016/0022-2836(90)90194-Q.

Arata, T., M. Nakamura, H. Akahane, T. Aihara, S. Ueki, K. Sugata, H. Kusuhara, M. Morimoto, and Y. Yamamoto. 2003. Orientation and motion of myosin light chain and troponin in reconstituted muscle fibers as detected by ESR with a new bifunctional spin label. *Adv Exp Med Biol*. 538:279-283; discussion 284.

Baker, J.E., I. Brust-Mascher, S. Ramachandran, L.E. LaConte, and D.D. Thomas. 1998. A large and distinct rotation of the myosin light chain domain occurs upon muscle contraction. *In* Proc Natl Acad Sci U S A. 2944-2949.

Binder, B.P., S. Cornea, A.R. Thompson, R.J. Moen, and D.D. Thomas. 2015. High-resolution helix orientation in actin-bound myosin determined with a bifunctional spin label. *Proc Natl Acad Sci USA*. 112:7972-7977. doi:10.1073/pnas.1500625112.

Binder, B.P., A.R. Thompson, and D.D. Thomas. 2018. High-resolution models of actin-bound myosin from EPR of a bifunctional spin label. *bioRxiv*.458257.

Brack, A.S., B.D. Brandmeier, R.E. Ferguson, S. Criddle, R.E. Dale, and M. Irving. 2004. Bifunctional rhodamine probes of Myosin regulatory light chain orientation in relaxed skeletal muscle fibers. *Biophys J*. 86:2329-2341. doi:10.1016/S0006-3495(04)74290-3.

Chen, L.F., H. Winkler, M.K. Reedy, M.C. Reedy, and K.A. Taylor. 2002. Molecular modeling of averaged rigor crossbridges from tomograms of insect flight muscle. *J Struct Biol*. 138:92-104.

Cooke, R., M.S. Crowder, and D.D. Thomas. 1982. Orientation of spin labels attached to cross-bridges in contracting muscle fibres. *Nature*. 300:776-778.

Enkhbayar, P., S. Damdinsuren, M. Osaki, and N. Matsushima. 2008. HELFIT: Helix fitting by a total least squares method. *Comput Biol Chem*. 32:307-310. doi:DOI 10.1016/j.compbiolchem.2008.03.012.

Fleissner, M.R., M.D. Bridges, E.K. Brooks, D. Cascio, T. Kalai, K. Hideg, and W.L. Hubbell. 2011. Structure and dynamics of a conformationally constrained nitroxide side chain and applications in EPR spectroscopy. *Proc Natl Acad Sci USA*. 108:16241-16246. doi:10.1073/pnas.1111420108.

Fujii, T., and K. Namba. 2017. Structure of actomyosin rigour complex at 5.2 A resolution and insights into the ATPase cycle mechanism. *Nat Commun*. 8:13969. doi:10.1038/ncomms13969.

Fusi, L., Z. Huang, and M. Irving. 2015. The Conformation of Myosin Heads in Relaxed Skeletal Muscle: Implications for Myosin-Based Regulation. *Biophysical Journal*. 109:783-792. doi:10.1016/j.bpj.2015.06.038.

Goldman, S.A., G.V. Bruno, and J.H. Freed. 1972. Estimating slow-motional rotational correlation times for nitroxides by electron spin resonance. *The Journal of Physical Chemistry*. 76:1858-1860. doi:10.1021/j100657a013.

Guhathakurta, P., E. Prochniewicz, and D.D. Thomas. 2015. Amplitude of the actomyosin power stroke depends strongly on the isoform of the myosin essential light chain. *Proc Natl Acad Sci U S A*. 112:4660-4665. doi:10.1073/pnas.1420101112.

Her, C., A.R. Thompson, C.B. Karim, and D.D. Thomas. 2018. Structural dynamics of calmodulin-ryanodine receptor interactions: electron paramagnetic resonance using stereospecific spin labels. *Sci Rep*. 8:10681. doi:10.1038/s41598-018-29064-8.

Himmel, D.M., S. Gourinath, L. Reshetnikova, Y. Shen, A.G. Szent-Gyorgyi, and C. Cohen. 2002. Crystallographic findings on the internally uncoupled and near-rigor states of myosin: further insights into the mechanics of the motor. *Proc Natl Acad Sci U S A*. 99:12645-12650.

Houdusse, A., A.G. Szent-Gyorgyi, and C. Cohen. 2000. Three conformational states of scallop myosin S1. *Proc Natl Acad Sci U S A*. 97:11238-11243.

Humphrey, W., A. Dalke, and K. Schulten. 1996. VMD: Visual molecular dynamics. *J Mol Graph Model*. 14:33-38. doi:Doi 10.1016/0263-7855(96)00018-5.

Irving, M. 2017. Regulation of Contraction by the Thick Filaments in Skeletal Muscle. *Biophys J*. 113:2579-2594. doi:10.1016/j.bpj.2017.09.037.

Knowles, A.C., R.E. Ferguson, B.D. Brandmeier, Y.B. Sun, D.R. Trentham, and M. Irving. 2008. Orientation of the essential light chain region of myosin in relaxed, active, and rigor muscle. *Biophysical Journal*. 95:3882-3891. doi:10.1529/biophysj.108.131508.

Mello, R.N., and D.D. Thomas. 2012. Three distinct actin-attached structural states of myosin in muscle fibers. *Biophys J*. 102:1088-1096. doi:S0006-3495(12)00054-9 [pii] 10.1016/j.bpj.2011.11.4027.

Muretta, J.M., J.A. Rohde, D.O. Johnsrud, S. Cornea, and D.D. Thomas. 2015. Direct real-time detection of the structural and biochemical events in the myosin power stroke. *Proc Natl Acad Sci U S A*. 112:14272-14277. doi:10.1073/pnas.1514859112.

Nelson, W.D., S.E. Blakely, Y.E. Nesmelov, and D.D. Thomas. 2005. Site-directed spin labeling reveals a conformational switch in the phosphorylation domain of smooth muscle myosin. *Proc Natl Acad Sci U S A*. 102:4000-4005.

Nogara, L., N. Naber, E. Pate, M. Canton, C. Reggiani, and R. Cooke. 2016. Spectroscopic Studies of the Super Relaxed State of Skeletal Muscle. *PLoS ONE*. 11:e0160100. doi:10.1371/journal.pone.0160100.

Prochniewicz, E., D.A. Lowe, D.J. Spakowicz, L. Higgins, K. O'Conor, L.V. Thompson, D.A. Ferrington, and D.D. Thomas. 2008. Functional, structural, and chemical changes in myosin associated with hydrogen peroxide treatment of skeletal muscle fibers. *Am J Physiol Cell Physiol*. 294:C613-626.

Rayes, R.F., T. Kalai, K. Hideg, M.A. Geeves, and P.G. Fajer. 2011. Dynamics of tropomyosin in muscle fibers as monitored by saturation transfer EPR of bi-functional probe. *PLoS ONE*. 6:e21277. doi:10.1371/journal.pone.0021277.

Rohde, J.A., D.D. Thomas, and J.M. Muretta. 2017. Heart failure drug changes the mechanoenzymology of the cardiac myosin powerstroke. *Proc Natl Acad Sci U S A*. 114:E1796-E1804. doi:10.1073/pnas.1611698114.

Romano, D., B.D. Brandmeier, Y.B. Sun, D.R. Trentham, and M. Irving. 2012. Orientation of the N-terminal lobe of the myosin regulatory light chain in skeletal muscle fibers. *Biophys J*. 102:1418-1426. doi:10.1016/j.bpj.2012.02.010.

Schmitz, H., M.C. Reedy, M.K. Reedy, R.T. Tregear, H. Winkler, and K.A. Taylor. 1996. Electron tomography of insect flight muscle in rigor and AMPPNP at 23 degrees C. *J Mol Biol*. 264:279-301. doi:10.1006/jmbi.1996.0641.

Thomas, D.D., and R. Cooke. 1980. Orientation of spin-labeled myosin heads in glycerinated muscle fibers. *Biophys J*. 32:891-906.

Thomas, D.D., D. Kast, and V.L. Korman. 2009. Site-directed spectroscopic probes of actomyosin structural dynamics. *Annu Rev Biophys*. 38:347-369.

Thomas, D.D., J.M. Muretta, B.A. Colson, R.N. Mello, and D. Kast. 2012. 4.12 Spectroscopic Probes of Muscle Proteins. *In* Comprehensive Biophysics. H.E. Editor-in-Chief: Edward, editor. Elsevier, Amsterdam. 226-250.

Thompson, A.R., B.P. Binder, J.E. McCaffrey, B. Svensson, and D.D. Thomas. 2015. Bifunctional Spin Labeling of Muscle Proteins: Accurate Rotational Dynamics, Orientation, and Distance by EPR. *Methods in enzymology*. 564:101-123. doi:10.1016/bs.mie.2015.06.029.

Thompson, A.R., N. Naber, C. Wilson, R. Cooke, and D.D. Thomas. 2008. Structural dynamics of the actomyosin complex probed by a bifunctional spin label that cross-links SH1 and SH2. *Biophys J*. 95:5238-5246.